**Inelastic nu and nubar scattering on nuclei and strangeness of the nucleon**

(Article begins on next page)

14 December 2021

# Inelastic $\nu$ and $\bar{\nu}$ scattering on nuclei and "strangeness" of the nucleon

W.M. Alberico [a], M.B. Barbaro [a], S.M. Bilenky [b,c], J.A. Caballero [d,1],
C. Giunti [a], C. Maieron [a], E. Moya de Guerra [d], J.M. Udías [d,2]

[a] INFN, Sezione di Torino and Dipartimento di Fisica Teorica, Università di Torino, Via P. Giuria 1, 10125
Torino, Italy
[b] Joint Institute for Nuclear Research, Dubna, Russia
[c] Technion, Physics Department, 320000 Haifa, Israel
[d] Instituto de Estructura de la Materia, CSIC, Serrano 123, E-28006 Madrid, Spain

## Abstract

Possibilities to extract information on the strange form factors of the nucleon from neutrino (anti-neutrino) inelastic scattering on nuclei, in an energy range from 200 MeV to 1 GeV and more, are investigated in detail. All calculations are performed within two relativistic independent particle models (Fermi gas and shell model); the final state interactions of the ejected nucleon are taken into account through relativistic optical model potentials. We have shown that the values of the cross sections significantly depend on the nuclear model (especially in the lower energy range). However, the NC/CC neutrino–anti-neutrino asymmetry in a medium–high energy range shows a rather small dependence on the model and allows to disentangle different values of the parameters that characterize the strange form factors. We have calculated also the ratio of the cross sections for inelastic NC scattering of neutrinos on nuclei, with the emission of a proton and of a neutron. Our calculations show that at high neutrino energy this ratio depends rather weakly on the nuclear model and confirm previous conclusions on the rather strong dependence of this ratio upon the axial strange form factors; however, at $E_\nu \leqslant 200$ MeV, the FSI are found to significantly affect the ratio. © 1997 Elsevier Science B.V.

*PACS:* 12.15.mn; 25.30.Pt; 13.60.Hb; 14.20.Dh; 14.65.Bt
*Keywords:* Neutrino–nucleus scattering; Strange form factors; Nuclear model effects

[1] Permanent address: Dpto. de Física Atómica, Molecular y Nuclear, Universidad de Sevilla, Apdo. 1065, E-41080 Sevilla, Spain.
[2] Present address: Dpto. de Física Atómica, Molecular y Nuclear,
Fac. de CC. Físicas, Univ. Complutense de Madrid, Ciudad Universitaria, E-28040 Madrid, Spain.

## 1. Introduction

The elastic and inelastic NC scattering of neutrinos (and anti-neutrinos) on nucleons and nuclei can be an important tool to determine the structure of the hadronic weak neutral current. In the present paper we will consider in detail what kind of information about the matrix elements of the axial and vector *strange* currents can be obtained from the investigation of these neutrino processes.

The one-nucleon matrix element of the axial strange current,

$$\langle p | \bar{s}\gamma^{\alpha}\gamma_5 s | p \rangle = 2M s^{\alpha} g_A^s ,$$

($p$ is the nucleon momentum, $s^{\alpha}$ the spin vector, $M$ is the nucleon mass and $g_A^s$ is the strange axial constant) has received new attention (see Refs. [1–3]) after the measurements of the polarized structure function $g_1$ of the proton performed by the EMC [4] collaboration and by the latest experiments done at CERN [5] and SLAC [6]. According to the theoretical analysis of these data the value $g_A^s = -0.10 \pm 0.03$ has been set [7]. Apart from experimental uncertainties, however, this value is affected by several assumptions, like the small $x$ behaviour of the polarized structure function of the proton(see for example Ref. [8]) and the assumption of exact SU(3) symmetry [9].

The strange vector current, instead, has been somewhat investigated in the context of parity violating electron scattering, where polarized electron beams are employed to disentangle the tiny electromagnetic-weak interference cross section. The existing measurements [10] do not allow to fix up the so-called strange magnetic moment of the nucleon, leaving uncertainties even on its sign.

These facts point to the importance of exploiting other methods for the determination of the matrix elements of the strange vector and axial currents.

It has been pointed out in a preceding work [3] that measurements of the asymmetry:

$$\mathcal{A}_N(Q^2) = \frac{\left(d\sigma/dQ^2\right)_{\nu N}^{\text{NC}} - \left(d\sigma/dQ^2\right)_{\bar{\nu} N}^{\text{NC}}}{\left(d\sigma/dQ^2\right)_{\nu n}^{\text{CC}} - \left(d\sigma/dQ^2\right)_{\bar{\nu} p}^{\text{CC}}} , \tag{1.1}$$

could allow an unambiguous determination of the presence of the magnetic and/or axial strange form factors of the nucleon $N$. The numerator of Eq. (1.1) contains the difference between the elastic $\nu(\bar{\nu}) - N$ neutral current (NC) scattering cross sections, while in the denominator the difference of the cross sections of the charged current (CC) processes $\nu_{\mu}(\bar{\nu}_{\mu}) + n(p) \rightarrow \mu^-(\mu^+) + p(n)$ is considered. As it is shown in Ref. [3], using the standard model expressions for the nucleonic neutral and charged weak currents (the former including strange currents as well) the expression of the asymmetry reads:

$$\mathcal{A}_{p(n)} = \frac{1}{4 |V_{ud}|^2} \left( \pm 1 - \frac{F_A^s}{F_A} \right) \left( \pm 1 - 2\sin^2\theta_W \frac{G_M^{p(n)}}{G_M^3} - \frac{G_M^s}{2 G_M^3} \right) . \tag{1.2}$$

where $G_M^{p(n)}(Q^2)$ is the magnetic form factor of the proton (neutron), $G_M^3(Q^2) = (G_M^p - G_M^n)/2$ is the isovector nucleon magnetic form factor, $F_A(Q^2)$ the CC axial form

factor, $V_{ud}$ is the element of the CKM mixing matrix and $\theta_W$ is the Weinberg angle. In addition to these quantities, which are relatively well known, the strange axial ($F_A^s$) and magnetic ($G_M^s$) form factors enter directly into (1.2) and could be measured. In the above $-Q^2 = q^2 = q_0^2 - \boldsymbol{q}^2$ is the four-momentum transfer square.

Several present (and future [see for example Ref. [11]]) neutrino experiments employ complex nuclei as a target. Thus it is important to analyze the scattering cross sections for inelastic $\nu(\overline{\nu})$–nucleus processes.

In this work we consider the following reactions:

$$\nu_\mu(\overline{\nu}_\mu) + A \longrightarrow \nu_\mu(\overline{\nu}_\mu) + N + (A - 1) \qquad \text{(NC)}, \qquad (1.3)$$

$$\nu_\mu(\overline{\nu}_\mu) + A \longrightarrow \mu^-(\mu^+) + p(n) + (A - 1) \qquad \text{(CC)}, \qquad (1.4)$$

where $A$ represents a nucleus with mass number $A$. We perform a thorough analysis of the influence of various nuclear effects on the relative cross sections: the main task is to investigate the possibility of extracting relevant information on the strange form factors.

The theoretical estimates of the cross sections for the processes (1.3) and (1.4) are obviously affected by the nuclear model employed for the description of the nucleonic dynamics: since the effect of strange form factors is believed to be at most of the order of 10–15%, the uncertainty stemming from the specific nuclear model employed must be constrained within a few percent, otherwise the analysis of strangeness in nuclei becomes hopeless.

An additional complication of neutrino experiments concerns the poor knowledge of the kinematical variables at the lepton vertex. For NC processes the final neutrino cannot be detected at all, whereas for the CC ones the final charged lepton can be detected and its energy and momentum could be in principle measured. However, in both cases the energy momentum balance cannot be precisely determined at the lepton vertex because of the lack of monochromatic neutrino beams.

In these experiments, the energy-momentum of the ejected nucleon can be measured but, as the initial nucleon is bound in the target nucleus and the ejected nucleon interacts with the residual nucleus (the so called final state interactions, FSI), the energy-momentum balance occurring at the weak interaction vertex is not unambiguously determined.

Here we have considered the inelastic neutrino (anti-neutrino)–nucleus cross section at intermediate/large energy transfers for both NC and CC processes. We compare the results obtained within two typical nuclear models, the relativistic Fermi gas (RFG) and a relativistic shell model (RSM), which have been widely tested in the past for, e.g. inelastic electron–nucleus scattering. These models can be viewed as two rather extreme descriptions of the nuclear structure in the framework of the independent particle approach: while the RFG is a very schematic model that just takes into account the average kinetic energy of the nucleons in the nuclear medium, the RSM accounts for very detailed single-particle properties.

Neutrino–nucleus scattering has been considered in previous works by Horowitz and collaborators [12] both for neutral current reactions within the RFG and for

charged current reactions using a relativistic meson–nucleon model with Random-Phase-Approximation (RPA) corrections and momentum dependent self-consistent mean field. [13]. According to their conclusions RFG seems to be adequate at relatively high momentum transfers, in agreement with Singh and Oset [14], who found (non-relativistic) RPA corrections to be large only at low momentum transfers. The sensitivity of neutrino-nucleus NC cross sections to the model description of the nuclear dynamics has been first investigated by Barbaro et al. [15]. The RSM used here has been successfully tested against precise data on coincidence elastic electron–nucleus scattering [16,17]. The same model has also been tested against data on separated longitudinal/transverse structure functions at the quasi-elastic peak [18,19]. From the above mentioned studies one can extract a fair indication of the reliability of these models in different kinematical regions.

We will show here, and this is our main result, that the information on strange form factors which can be extracted from ratios of cross sections [like the nuclear analogous of the asymmetry (1.1)] is weakly affected by the different nuclear dynamics of the models even in cases where the nuclear model effects are sizeable in the evaluation of the separated cross sections. In particular the important effects of final state interactions are discussed here.

The explicit description of the models employed for the calculation of the $\nu(\bar{\nu})$–nucleus cross sections is introduced in Section 2, while in Section 3 we discuss the numerical results together with the implications for the possibility of measuring the strange form factors of the nucleon. The influence of Coulomb corrections on the charged current cross sections and of the interaction of the ejected nucleon with the residual nucleus is thoroughly examined and found to be not negligible, even for the ratios of cross sections considered here.

## 2. Formalism

For the description of the nuclear structure we employ here two independent particle models: the Fermi gas and the Shell Model, both of them in a relativistic version, which occurs to be more appropriate when the involved energy transfers are of the order of several hundreds MeV. In both cases it is assumed that the incoming neutrino (or anti-neutrino) interacts with a single nucleon, the remaining $A - 1$ being spectators.

Let us start by fixing up the kinematics of the process, which is illustrated in Fig. 1: the scattering plane $(x, z)$ is determined by the initial $(k)$ and final $(k')$ lepton momenta, the initial nucleus being at rest, and contains the momentum transfer $q = k - k'$. In the Impulse Approximation (IA) the intermediate boson with momentum $q$ is absorbed by a single nucleon with momentum $p$ inside the nucleus, which is then scattered to a final state with momentum $p_N$ (possibly after strong interactions with the residual nucleus): $p_N$ forms an angle $\gamma$ with $q$, while $\phi_N$ is the angle between the scattering plane and the one containing $q$ and $p_N$.

The exclusive cross sections we are interested in are generated, in lowest order of
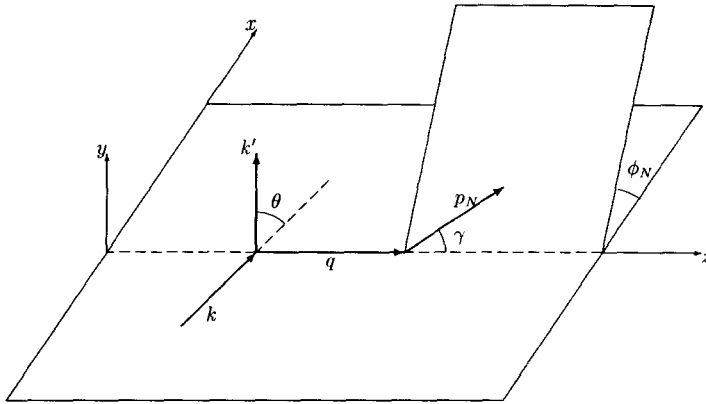
Fig. 1. The two scattering planes involved in the process: the initial and final neutrino momenta $(k, k')$ are in the $(x, z)$ plane; the outgoing nucleon $(p_N)$ in the inclined plane.
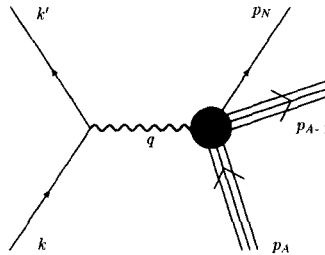


Fig. 2. Schematic representation for the amplitude, in Born approximation, of the neutrino-nucleus scattering.

the electroweak interaction, by the Feynman amplitude associated with the diagram of Fig. 2, where the hadronic final state is identified by the four-momenta of the ejected nucleon $(p_N)$ and of the daughter, $A - 1$ nucleus $(p_{A-1})$.

We consider the initial nucleus in its ground state $\Psi_A$ (at rest in the laboratory frame), while the final nuclear system will be described by the product of the knocked out nucleon wavefunction $\psi_N(p_N, s_N)$ and the residual nucleus state, $\Psi_{A-1}$, both of them being chosen within suitable model wavefunctions, which will be discussed below.

The nuclear current operator is the sum of single nucleon (one-body) currents. For the initial and final nuclear wavefunctions an independent particle model (IPM) is employed; then the exact nuclear current matrix elements can be formally written by using an *effective* current operator (see for example Ref. [20])

$$J_A^\mu = \langle \Psi_{A-1}^{IPM} \psi_N(p_N, s_N) | \hat{J}_{eff}^\mu | \Psi_A^{IPM} \rangle , \qquad (2.1)$$

where all the complexities inherent to the use of *exact* wave functions have been incorporated in the unknown effective current operator, that in general should be a rather complicated many-body operator. The matrix elements of the current are evaluated in the Impulse Approximation (IA), where the effective current operator is substituted by the *free* one-body nuclear current operator
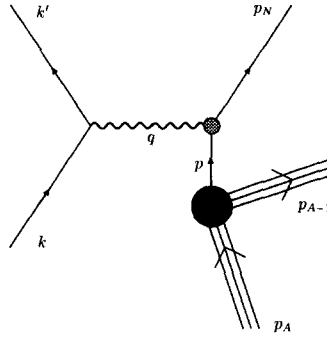
Fig. 3. Representation of the $\nu$-nucleus scattering in the Impulse Approximation.

$$\hat{J}^{\mu}_A = \sum_{k=1}^{A} \hat{J}^{\mu}_k ,$$

(2.2)

$\hat{J}^{\mu}_k$ being either the neutral or the charged single nucleon weak current operator; it is assumed to be on shell, as for the interaction in free space. This might be a rather crude approximation depending upon the kinematical conditions of the reaction under investigation. For the fairly large neutrino energies (and energy transfers) we are interested here, the IA is expected to be a reliable approximation [21].

We will now consider in more details the two independent particle models employed here, namely the relativistic Fermi gas and a relativistic shell model: they entail a quite different description of the nuclear structure and should allow a serious test of the influence of the nuclear model on the quantities under investigation.

## 2.1. Relativistic Fermi gas (RFG)

In this paragraph we present the relevant formalism used to express the NC and CC inelastic scattering cross sections for the processes (1.3) and (1.4) within a relativistic Fermi gas model for the nuclear target. We remind that a relativistic description of the single nucleon states (and currents) has proved to be of some relevance when the energy-momentum transferred to the nuclear system exceeds about 0.5 GeV. [22]

Within the framework of the RFG we shall restrict ourselves to the Plane Wave Impulse Approximation (PWIA), which does not take into account the interaction between the knocked out nucleon and the residual nucleus, as it is illustrated in Fig. 3. In this case three-momentum conservation in the laboratory system (where the initial nucleus is at rest) implies $p_{A-1} = -p$, with $p$ being the momentum of the struck nucleon before the interaction with the leptonic current. In the naive FG, nucleons inside the Fermi sea are on the mass-shell, with $p_0 = \sqrt{p^2 + M^2}$. However, it is possible, without major modifications of the approach, to account for an average, constant binding energy of the nucleon $-\epsilon_{\mathrm{B}}$, by replacing $p_0 \longrightarrow p_0 - \epsilon_{\mathrm{B}}$.

The outgoing nucleon, instead, is obviously assumed to be on shell, with energy $E_N = \sqrt{p_N^2 + M^2} \equiv T_N + M$, $T_N$ being its kinetic energy and $M$ the nucleon mass. We

notice that in PWIA the relation $q = p_N - p$ also holds.

The phase-space of the final states for the neutrino–nucleus scattering process is defined by the three-momenta of the outgoing lepton, nucleon and daughter nucleus: the latter however is not detected and thus one has to integrate the differential cross section stemming from the amplitude represented in Fig. 3 over $p_{A-1}$ or, according to the above considerations, over the struck nucleon momentum $p$, whose range is constrained within the occupied levels in the Fermi sphere ($|p| \leqslant p_F$, $p_F$ being the Fermi momentum).

We thus write the $\nu$–nucleus differential cross section with respect to the energy and angles of the ejected nucleon as follows

$$\left(\frac{d^2\sigma}{dE_N \, d\Omega_N}\right)_{\nu(\bar{\nu})A} = \frac{G_F^2}{(2\pi)^2} \frac{V}{(2\pi)^3} \frac{|p_N|}{4k_0} \int \frac{d^3k'}{k_0'} \frac{d^3p}{p_0} \delta\left(k_0 - k_0' + p_0 - E_N\right)$$

$$\times \delta^{(3)}\left(k - k' + p - p_N\right) \theta(p_F - |p|)\theta(|p_N| - p_F)$$

$$\times \left(L^{\mu\nu} \pm L_5^{\mu\nu}\right) w_{\mu\nu}^{s.n.}, \tag{2.3}$$

where $V$ is the nuclear volume,[3] $L^{\mu\nu}$ and $L_5^{\mu\nu}$ are the symmetric and antisymmetric parts, respectively, of the leptonic tensor,

$$L^{\mu\nu} = k^\mu k'^\nu + k'^\mu k^\nu - g^{\mu\nu} k \cdot k', \tag{2.4}$$

$$L_5^{\mu\nu} = i\epsilon^{\mu\nu\rho\sigma} k_\rho k'_\sigma, \tag{2.5}$$

and the plus (minus) sign refer to neutrino (anti-neutrino) scattering. Finally, $w_{\mu\nu}^{s.n.}$ is the single nucleon hadronic tensor:

$$w_{\mu\nu}^{s.n.} = \sum_{s,s_N} \langle p_N, s_N | \hat{J}_\mu | p, s \rangle \langle p, s | \hat{J}_\nu^\dagger | p_N, s_N \rangle. \tag{2.6}$$

In the above $\hat{J}_\mu$ is the weak nucleonic current, with matrix elements

$$\langle p_N, s_N | \hat{J}_\mu | p, s \rangle = \overline{U}_{s_N}(p_N) \Gamma_\mu U_s(p)$$

$$\equiv \overline{U}_{s_N}(p_N) \left[ \gamma_\mu F_V(Q^2) + \frac{i}{2M}\sigma_{\mu\alpha}q^\alpha F_M(Q^2) + \gamma_\mu\gamma_5 F_A(Q^2) - q_\mu\gamma_5 F_P(Q^2) \right] U_s(p),$$

$$\tag{2.7}$$

where the vector ($F_V$), magnetic ($F_M$) and axial ($F_A$) nucleonic form factors have to be specified, according whether one needs to consider neutral or charged processes and $Q^2 = -q^2$, being $q = p_N - p$. The pseudoscalar component ($F_P$) concerns only charged currents; in any case it does not contribute to *differences* of neutrino and anti-neutrino cross-sections, as the ones we are interested in for constructing an asymmetry like (1.1).

---

[3] Within the Fermi gas model the volume of the system can be re-expressed, via the relation $Z/V = N/V = p_F^3/3\pi^2$ (we consider here only $N = Z$ nuclei), in terms of the number of protons ($Z$) or neutrons ($N$) which enter into play in the specific process; at the same time the nucleonic form factors in the hadronic tensor will be specified as the ones of the corresponding nucleon (proton or neutron, respectively).

By inserting (2.7) into (2.6) one gets the general structure ($X_\mu = p_\mu - (p \cdot q)q_\mu/q^2$):

$$w_{\mu\nu}^{s.n.} = 8M^2 \left\{ -W_1 \left( g_{\mu\nu} - \frac{q_\mu q_\nu}{q^2} \right) + \frac{W_2}{M^2} X_\mu X_\nu + \frac{W_3}{M^2} i\epsilon_{\mu\nu\alpha\beta} p^\alpha q^\beta + \frac{W_4}{M^2} q_\mu q_\nu \right\}, \quad (2.8)$$

with

$$
\begin{aligned}
W_1 &= -\frac{q^2}{4M^2} \left[ (F_V + F_M)^2 + F_A^2 \right] + F_A^2, \\
W_2 &= F_V^2 - \frac{q^2}{4M^2} F_M^2 + F_A^2, \\
W_3 &= F_A (F_V + F_M), \\
W_4 &= -\frac{M^2}{q^2} F_A^2 + \frac{p \cdot q}{2} F_P^2 + M F_P F_A,
\end{aligned}
\qquad (2.9)
$$

where the on-shell condition ($p^2 = M^2$) for the struck nucleon inside the Fermi sea has been exploited.

Then the $\nu(\bar{\nu})$-nucleus cross section is expressed, in the RFG model, as follows:

$$
\begin{aligned}
\left( \frac{d^2\sigma}{dE_N \, d\Omega_N} \right)_{\nu(\bar{\nu})A} = {} & \frac{G_F^2}{(2\pi)^2} \frac{V}{(2\pi)^3} \frac{|\boldsymbol{p}_N|}{4k_0} \theta(|\boldsymbol{p}_N| - p_F) \\
& \times \int \frac{d^3k' \, d^3p}{k_0' \, p_0} \delta \left( k_0 - k_0' + p_0 - E_N \right) \\
& \times \delta^{(3)} \left( \boldsymbol{k} - \boldsymbol{k}' + \boldsymbol{p} - \boldsymbol{p}_N \right) \theta(p_F - |\boldsymbol{p}|) \\
& \times 8M^2 \left\{ 2k \cdot k' W_1 + \frac{W_2}{M^2} \left[ 2(k \cdot p)(k' \cdot p) - M^2 (k \cdot k') \right] \right. \\
& \pm \frac{2W_3}{M^2} \left( k' \cdot p + k \cdot p \right) k \cdot k' \\
& \left. + m_l^2 \left[ W_1 \frac{k \cdot k'}{q^2} + \frac{W_2}{M^2} \left( \frac{k \cdot k'}{4} - k \cdot p \right) \mp \frac{2W_3}{M^2} k \cdot p + \frac{W_4}{M^2} k \cdot k' \right] \right\},
\end{aligned}
$$
$$(2.10)$$

where the upper (lower) sign refers to $\nu(\bar{\nu})$ induced processes. Obviously terms proportional to the final lepton mass ($m_l$) only come into play for CC processes; they are derived in (2.10) by exploiting the condition $k'^2 = m_l^2$ (with $m_l = 0$ for NC, $m_l = m_\mu$ for CC).

The integration over $\boldsymbol{k}'$ can be carried out by using the delta function, while $\boldsymbol{p}$ can be (numerically) integrated by taking into account the kinematical conditions of the scattering under investigation. We will consider a definite value for $k$: usually the $\nu$ beam is not monochromatic and the analysis of real experimental data will require an integration over the neutrino energy spectrum; $\boldsymbol{p}_N$ is measured by detecting the outgoing nucleon. This fixes the four-vector

$$\epsilon = p_N - k,$$

and the Mandelstam variable

$$u = \epsilon^2 = (k - p_N)^2 = M^2 - 2p_N \cdot k \,.$$

Let us define $\theta_N$ as the angle between $k$ and $p_N$ (remind that $|k|^2 = k_0^2$):

$$|\epsilon| = |p_N - k| = \left\{ p_N^2 + k_0^2 - 2|p_N|k_0 \cos \theta_N \right\}^{1/2} \,.$$

Further, by assuming $\epsilon$ along the $z$-axis, we call $\theta_p$ the angle between $p$ and $\epsilon$ ($\cos \theta_p = \hat{p} \cdot \hat{\epsilon}$) and rewrite the remaining energy-conserving delta function in terms of $\cos \theta_p$ as follows:

$$\frac{1}{k_0'} \delta \left( k_0 - k_0' + p_0 - E_N \right) = \frac{1}{|p| \, |\epsilon|} \delta(\cos \theta_p - y_0) \,,$$

having set

$$y_0 = \frac{1}{|p| \, |\epsilon|} \left( \epsilon_0 p_0 \cdot - \frac{M^2 + u - m_l^2}{2} \right) \tag{2.11}$$

The last expression allows to perform the integral over $d \cos \theta_p$: this already eliminates (at least partially) the explicit dependence upon $q^2$ of the integrand, though it will be formally maintained in the structure factors $W_i$. Again the leptonic mass appearing in (2.11) concerns only the charged current processes in the denominator of the asymmetry: for neutral current $\nu$-nucleus cross sections, obviously, it has to be set equal to zero.

The cross section (2.10) can be rewritten as:

$$\left( \frac{d^2\sigma}{dE_N \, d\Omega_N} \right)_{\nu(\bar{\nu})A} = \frac{G_F^2}{(2\pi)^2} \frac{V}{(2\pi)^3} \frac{2M^2|p_N|}{k_0|\epsilon|} \theta \left( |p_N| - p_F \right) \int\limits_0^{p_F} d|p| \frac{|p|}{p_0}$$

$$\times \int\limits_{-1}^{1} d \cos \theta_p \delta(\cos \theta_p - y_0) \int\limits_0^{2\pi} d\phi \left\{ \mathcal{I}_1 + \mathcal{I}_2 \pm \mathcal{I}_3 + \mathcal{I}_4 \right\} , \tag{2.12}$$

where, after some algebra, the functions $\mathcal{I}_i$ are defined as follows:

$$\mathcal{I}_1 = -W_1(q^2) \left( M^2 - u - 2k \cdot p \right) \left( 1 + \frac{m_l^2}{2q^2} \right) , \tag{2.13}$$

$$\mathcal{I}_2 = \frac{W_2(q^2)}{M^2} \left[ \frac{M^2}{2} \left( M^2 - u \right) - u(k \cdot p) + \frac{m_l^2}{4} \left( k \cdot p - \frac{M^2 - u}{2} \right) \right] , \tag{2.14}$$

$$\mathcal{I}_3 = \frac{2W_3(q^2)}{M^2} \left[ (k \cdot p) \left( k \cdot p - \frac{1}{2} m_l^2 \right) - \frac{1}{4} \left( M^2 - u \right) \left( M^2 - u + m_l^2 \right) \right] , \tag{2.15}$$

$$\mathcal{I}_4 = \frac{W_4(q^2)}{M^2} m_l^2 \left[ k \cdot p - \frac{1}{2} \left( M^2 - u \right) \right] . \tag{2.16}$$

In the above $q^2 = M^2 - u + m_l^2 - 2k \cdot p$ and the scalar product $k \cdot p$ is a non-trivial function of $\cos \theta_p$ and $\phi$. As already stated, in the previous formulas we have employed the on-shell condition, $p_0 = \sqrt{M^2 + p^2}$, for the nucleon inside the Fermi sea; this condition, however, can be partly released in order to account for an average, constant

binding energy $\epsilon_B$ [12]. In this case the energy $p_0$ in the $\delta$-function in (2.3) must be replaced by $p_0 - \epsilon_B$. As we will show in the numerical results presented below, this "minor" modification makes the RFG cross sections (in the quasi-elastic kinematics considered here) much more realistic and closer to the shell model calculation.

Another correction, which refers only to the CC processes, stems from the distortion on the wavefunction of the final (charged) lepton due to its interaction with the Coulomb field of the (residual) nucleus. Still remaining in Born Approximation for the main scattering process, this Coulomb correction should be taken into account by replacing the plane wave describing the final lepton with an "exact" eigenfunction of the nuclear Coulomb field. This procedure, however, is somewhat complicated (see, for example, Refs. [16,23]): the main effects of the Coulomb distortion can be more easily accounted for by means of the prescription (which can be used both within the RFG and the RSM) described below.

The main point is to replace the plane wave, $e^{i k' \cdot r}$, of the outgoing lepton by:

$$\frac{|k'_{\text{eff}}|}{|k'|} e^{i k'_{\text{eff}} \cdot r} ,$$

where

$$k'_{\text{eff}} = k' \left( 1 \pm \frac{3}{2} \frac{Z\alpha}{R|k'|} \right) . \qquad (2.17)$$

In the above the plus (minus) refers to the lepton ($\mu^-$) and the antilepton ($\mu^+$), respectively, $Z$ is the number of protons and $R \simeq 1.2 A^{1/3}$ is the effective charge radius of the nucleus under investigation. This approximation has been tested within a non-relativistic approach in Ref. [24].

The substitution $k' \rightarrow k'_{\text{eff}}$ obviously affects the kinematics in the three-momentum conserving $\delta$-function and the phase space of the final lepton, but also the energy $k'_0$ of the outgoing lepton (still to be considered on the mass shell), once it is expressed in terms of $k'_{\text{eff}}$. We shall comment upon the Coulomb corrections on the CC cross-sections in the discussion of the numerical results.

Thus far we have considered double differential cross sections: however, to test the sensitivity to the presence of strange form factors, we will consider single differential cross sections with respect to the (kinetic) energy of the knocked out nucleon. The latter can be obtained from our previous formulas by further integrating over the solid angle $\Omega_N$. Formally:

$$\left( \frac{d\sigma}{dE_N} \right)_{\nu(\bar{\nu})A} = \left( \frac{d\sigma}{dT_N} \right)_{\nu(\bar{\nu})A} = \frac{G_F^2}{2\pi} \frac{V}{(2\pi)^3} \frac{2M^2|p_N|}{k_0|\epsilon|} \theta\left(|p_N| - p_F\right) \int_{-1}^{+1} d\cos\theta_N$$

$$\times \int_0^{p_F} \frac{d|p||p|}{p_0} \theta(1 - |y_0|) \int_0^{2\pi} d\phi \left\{ \mathcal{I}_1 + \mathcal{I}_2 + \mathcal{I}_3 + \mathcal{I}_4 \right\} \Big|_{\cos\theta_p = y_0} , \qquad (2.18)$$

Total cross sections (integrated over the final nucleon energy) will be utilized as well. They are defined as:

$$\sigma_{\nu(\bar{\nu})A} = \int dT_N \left(\frac{d\sigma}{dT_N}\right)_{\nu(\bar{\nu})A}. \tag{2.19}$$

In the above we have presented general formulas, which are valid both for NC and CC processes: for a specific calculation one should take care of the following remarks:

(i) in the case of NC cross-sections the form factors appearing in (2.9) will be denoted by $F_i^Z$ ($i = V, M, A$) (while $F_P$ does not contribute);

(ii) in the case of CC cross-sections the form factors will be $F_i^{CC}$ ($i = V, M, A, P$) and the additional replacement $G_F^2 \Longrightarrow G_F^2 |V_{ud}|^2$ is required.

### 2.2. Relativistic shell model

In this approach we shall use a relativistic shell model for the wavefunctions of the initial (target) and of the final (residual) nucleus, while we shall assume a final scattering state for the knocked out nucleon. Moreover the IA will be employed, as in the previous case. Thus the nuclear current matrix element $J_A^\mu$ for the process we are interested here, is computed as [see also Eq. (2.1)]

$$J_A^\mu = \left\langle \Psi_{A-1}^{SM}(P_{A-1})\psi_N(P_N, s_N) \left| \sum_{k=1}^{A} \hat{J}_k^\mu \right| \Psi_A^{SM}(P_A) \right\rangle, \tag{2.20}$$

where the (free) current operator is built up as in (2.2) and $P_A(P_{A-1})$ are the four-momenta of the initial (final) nucleus, respectively. The final state

$$|\Psi_{A-1}^{SM}(P_{A-1})\psi_N(P_N, s_N)\rangle$$

is a single-channel optical-model wave function constructed from the product of a final state for the $A - 1$ particles residual nucleus and either a plane wave (PWIA) or a distorted wave (DWIA) for the outgoing ejected nucleon. The initial nuclear state can be equivalently rewritten as $|\psi_B^{SM}, \Psi_{A-1}^{SM}(P_{A-1})\rangle$, denoting a (bound-state) single-particle shell model wave function coupled to the rest of the initial nucleus.

After performing the angular momentum algebra involved in the shell model description for the residual and target nuclei, the nuclear current can be expressed in terms of spectroscopic amplitudes $f_j(I_A, I_{A-1})$ times single-particle current matrix elements, $I_A(I_{A-1})$ being the angular momentum of the target (residual) nucleus.

The required single-particle matrix elements are of the form:

$$J_\mu(q) = \sqrt{V} \int d^3r \, e^{iq\cdot r} \, \overline{\psi}_{s_N}(p_N, r) \Gamma_\mu \psi_{B,\kappa}^{jm}(r), \tag{2.21}$$

where $\psi_{B,\kappa}^{jm}, \psi_{s_N}$ are the wave functions for the initial bound nucleon (with quantum numbers $j, m, \kappa$) and for the final outgoing nucleon (with momentum $p_N$), respectively;

$\Gamma_\mu$ is the same single-particle current operator for free nucleons, which was defined in Eq. (2.7).

We will consider first the so-called PWIA, thus neglecting the interaction in the final state (FSI) between the ejected nucleon and the residual nucleus; the single particle matrix elements of the current can then be computed as:

$$J_\mu(q) = \frac{1}{\sqrt{2E_N}} \overline{U}(p_N, s_N) \int dr \, e^{-ip\cdot r} \Gamma_\mu \psi_{B,\kappa}^{jm}(r) , \tag{2.22}$$

with $p = p_N - q$.

In this approximation the differential cross-section with respect to the energy of the ejected nucleon can be written as [25,26]

$$\frac{d\sigma^{SM}}{dE_N} = 4\pi |f_j(I_A, I_{A-1})|^2 \int dk'_0 \int d(\cos\theta) E_{A-1} \frac{1}{|q|} \left(\frac{d\sigma}{d\Omega}\right)^{Z^0/W^\pm}$$
$$\times \left[\omega_L \overline{W}_L + \omega_T \overline{W}_T + \omega_{TT'} \overline{W}_{TT'}\right] , \tag{2.23}$$

where the bars over the structure functions $W_i$ imply averages (sum) over the initial (final) nucleonic states:

$$\overline{W}_i = \frac{1}{2j+1} \sum_{m,m'} W_i .$$

In the previous expressions $q = k - k'$ is the 3-momentum transfer and $\theta$ is the scattering angle of the final lepton. $E_{A-1}$ is the energy of the residual nucleus, and $(d\sigma/d\Omega)^{Z^0/W^\pm}$ are Mott-like cross-sections that assume the following form for neutral and charged current processes:

$$\left(\frac{d\sigma}{d\Omega}\right)^{Z^0} = \frac{G_F^2}{2\pi^2} k_0'^2 \cos^2(\theta/2) , \tag{2.24}$$

$$\left(\frac{d\sigma}{d\Omega}\right)^{W^\pm} = 4|V_{ud}|^2 \frac{G_F^2}{2\pi^2} |k'|^2 . \tag{2.25}$$

For closed shell nuclei in the extreme shell model, we have $|f_j(I_A, I_{A-1})|^2 = 2j + 1$. When several shells contribute we just sum the corresponding cross-section for every shell.

The integrations in Eq. (2.23) are performed numerically. To compute the limits, one should keep in mind that $k_0 - k'_0 = \omega$, $\omega_{min} = M_{A-1} + E_N - M_A$ being the minimum required energy transfer; moreover the following kinematical constraints hold:

$$|P_{A-1} - p_N| \leqslant |q| \leqslant |P_{A-1} + p_N| , \tag{2.26}$$

$$|k - k'| \leqslant |q| \leqslant |k + k'| . \tag{2.27}$$

The remaining terms in Eq. (2.23) are the "kinematical" coefficients $\omega_L, \omega_T, \omega_{TT'}$ and the response functions $W_L, W_T, W_{TT'}$, which will be specified below.

In the case of neutral currents, since the mass of both the initial and final lepton is zero (so that $k_0 = |\mathbf{k}|, k_0' = |\mathbf{k}'|$) the expressions of the kinematical coefficients read:

$$\omega_L = 1 \,, \tag{2.28}$$

$$\omega_T = \tan^2(\theta/2) - \frac{q^2}{2\mathbf{q}^2} \,, \tag{2.29}$$

$$\omega_{TT'} = \pm 2 \tan(\theta/2) \sqrt{\tan^2(\theta/2) - q^2/\mathbf{q}^2} \,, \tag{2.30}$$

the minus (plus) sign referring to neutrino (anti-neutrino).

To write explicitly the structure functions we choose a coordinate system defined by the unit vectors $(\hat{q}, \hat{n}_\perp, \hat{n}_\parallel)$, where $\hat{n}_\perp$ is the direction perpendicular to the nucleon scattering plane (i.e. the plane defined by $\mathbf{q}$ and $\mathbf{p}_N$), and $\hat{n}_\parallel$ is a vector in the nucleon scattering plane perpendicular to $\mathbf{q}$ and $\hat{n}_\perp$. We write here the four-vector hadronic current as $J^\mu \equiv (\rho, \mathbf{J})$; then, according to the above definitions:

$$\mathbf{J} = J_q \hat{q} + J_\perp \hat{n}_\perp + J_\parallel \hat{n}_\parallel \,, \tag{2.31}$$

$$\hat{n}_\perp \equiv (-\sin \phi_N, \cos \phi_N, 0) \,, \tag{2.32}$$

$$\hat{n}_\parallel \equiv (\cos \phi_N, \sin \phi_N, 0) \,, \tag{2.33}$$

$$\mathbf{p}_N \equiv |\mathbf{p}_N|(\sin \gamma \cos \phi_N, \sin \gamma \sin \phi_N, \cos \gamma) \,, \tag{2.34}$$

where $\gamma, \phi_N$ are the scattering and azimuthal angles for the ejected nucleon (see also Fig. 1).

After integrating on the unobserved final nucleon angles, the structure functions can be rewritten in terms of the nuclear current components as follows:

$$W_L = |\rho|^2 + \frac{\omega^2}{\mathbf{q}^2}|J_q|^2 - \frac{\omega}{|\mathbf{q}|} 2 Re \, (\rho J_q^\dagger) \,, \tag{2.35}$$

$$W_T = |J_\parallel|^2 + |J_\perp|^2 \,, \tag{2.36}$$

$$W_{TT'} = Im \, (J_\parallel J_\perp^\dagger) \,. \tag{2.37}$$

For charged current reactions of type $(\nu_l, lN)$ or $(\overline{\nu}_l, \overline{l}N)$ with final lepton mass $m_l$, we obtain the same expression for $W_T$ and $W_{TT'}$, while

$$
\begin{aligned}
\omega_L W_L = \frac{1}{4k_0|\mathbf{k}'|} \Bigg\{ &\left[ (k_0 + k_0')^2 - |\mathbf{q}|^2 - m_l^2 \right] |\rho|^2 \\
&+ \left[ \frac{(k_0^2 - |\mathbf{k}'|^2)^2}{|\mathbf{q}|^2} - \omega^2 + m_l^2 \right] |J_q|^2 \\
&- \left[ \frac{2(k_0 + k_0')(k_0^2 - |\mathbf{k}'|^2)}{|\mathbf{q}|} - 2\omega|\mathbf{q}| \right] Re \, (\rho J_q^\dagger) \Bigg\} \,,
\end{aligned}
\tag{2.38}
$$

$$\omega_T = \frac{k_0|\mathbf{k}'|\sin^2 \theta}{2|\mathbf{k}|^2} - \frac{1}{2}\left( \frac{-k_0'}{|\mathbf{k}'|} + \cos \theta \right) \,, \tag{2.39}$$

$$\omega_{TT'} = \pm \frac{1}{|\boldsymbol{k}|} \left( \frac{k_0 k_0'}{|\boldsymbol{k}'|} + |\boldsymbol{k}'| - (k_0 + k_0') \cos\theta \right) . \tag{2.40}$$

In the expressions for the $TT'$ contribution, the upper and lower signs correspond to neutrino and anti-neutrino scattering, respectively. We have written the expressions for neutral and charged current simultaneously, but we have to keep in mind (as it was pointed out in the analogous situation for the RFG) that the current operator to be used in Eq. (2.22) will include different form-factors for neutral and charged current.

The bound nucleon wave functions are computed in a relativistic framework, as solutions of a Dirac equation with scalar and vector potentials. We use the wave functions obtained with the TIMORA code [27]. This code implements a self-consistent Hartree procedure with Mean Field solutions of a linear Lagrangian including nucleons and scalar ($\sigma$) vector-isoscalar ($\omega$) and vector–isovector ($\rho$) mesons. The free parameters of the lagrangian (the nucleon–meson coupling constants for the $\sigma, \omega$ and $\rho$ and the mass of the scalar particle) are adjusted to reproduce nuclear matter properties and the *rms* radius of $^{40}$Ca [28]. Several other lagrangians including a non-linear self-coupling of the scalar meson, with parameters adjusted to the binding energies and *rms* radii of magic nuclei are also being currently used [29,30]. The bound state wave functions obtained with these alternative models are not very different from the ones used here [31]. The solutions of the linear lagrangian used in this work well reproduce the observed cross-sections of the $(e, e'p)$ reactions in several nuclei without further adjustment [16,17].

We have also verified that the results for the cross-sections of this work are almost insensitive to the choice of the lagrangian used, providing that the same single-particle binding energies are used in the different models. As these ones determine the threshold of the cross-section for every shell, we have used the experimentally measured values of the binding energies.

Within this relativistic framework the bound state wave function for the initial nucleon, $\psi_{B,\kappa}^{jm}$, is a four-spinor with well defined angular momentum quantum numbers $j, m$ and $\kappa$ corresponding to the shell under consideration. We use four-spinors of the form

$$\psi_{B,\kappa}^{jm}(\boldsymbol{r}) = \begin{pmatrix} g_\kappa(r)\phi_\kappa^{jm}(\hat{r}) \\ if_\kappa(r)\phi_{-\kappa}^{jm}(\hat{r}) \end{pmatrix} \tag{2.41}$$

that are eigenstates of total angular momentum with eigenvalue $j = |\kappa| - 1/2$,

$$\phi_\kappa^{jm}(\hat{r}) = \sum_{m_\ell, s} \langle \ell \, m_\ell \tfrac{1}{2} s | jm \rangle Y_{\ell m_\ell}(\hat{r}) \chi_s , \tag{2.42}$$

with $\ell = \kappa$ for $\kappa > 0$, $\ell = -\kappa - 1$ for $\kappa < 0$. $f_\kappa$ and $g_\kappa$ are the solutions of the usual radial equations [32]. The normalization we use is $\int_V \psi_\kappa^{jm\dagger}(\boldsymbol{r})\psi_\kappa^{jm}(\boldsymbol{r}) \, d\boldsymbol{r} = 1$.

In the framework of the RSM we will consider two different situations for the ejected nucleon: in the first one, which compares with the RFG calculation, no interaction is taken into account between it and the residual nucleus (PWIA). Then the wave function for the outgoing nucleon is also a four-component spinor, obtained as a partial wave

expansion in configuration space of a plane wave, i.e. a solution of the *free* Dirac equation.

In the second case the FSI between the outgoing nucleon and the residual nucleus is accounted for by an appropriate Relativistic Optical Model potential (hereafter referred to as ROP), which is embodied in the Dirac Equation for the ejected nucleon (DWIA):

$$[i\boldsymbol{\alpha} \cdot \boldsymbol{\nabla} - \beta(M + U_S) + E - U_V - U_C]\,\psi(\boldsymbol{r}) = 0\,. \tag{2.43}$$

The scalar ($U_S$), vector ($U_V$) and Coulomb ($U_C$) components of the potential can be derived within the same meson-exchange relativistic model which is employed for the description of the bound nuclear states; more often, however, one utilizes phenomenological potentials, which are fitted to the elastic nucleon–nucleus scattering. In particular the real part of the (complex) optical potential is related with the elastic rescattering of the ejected nucleon, while the imaginary part accounts for the absorption of it into unobserved channels (or its re-absorption by the residual nucleus). The vector and scalar part of the ROP we employed here have the form:

$$U_V(r, E) = V_0(E)f_0(r, E) + i\left[W_0(E)g_0(r, E) + W_{0SP}(E)h_0(r, E)\right]\,, \tag{2.44}$$

$$U_S(r, E) = V_s(E)f_s(r, E) + i\left[W_s(E)g_s(r, E) + W_{sSP}(E)h_s(r, E)\right]\,, \tag{2.45}$$

where $f_i$ and $g_i$ ($i = 0, s$) are symmetrized Woods–Saxon functions, while the $h_i$ are derivatives of Woods–Saxon functions. The strengths $V_i, W_i$ (as well as the radii of the Woods–Saxon distributions) have an explicit energy dependence. This ROP corresponds to one of the energy-dependent parameterization of Cooper *et al.* [33] of Dirac optical potentials fitted to elastic proton scattering data in an extensive range of proton energies and mass number nuclei. The potential used in this work is the A-independent single nucleus parameterization for $^{12}C$ presented in Ref. [33]. The results obtained with the other choices for the optical potential contained in Ref. [33] are very similar to the ones presented here.

Once inserted the above ROP into the Dirac equation, the corresponding solutions read:

$$\psi_N(\boldsymbol{r}) = 4\pi\sqrt{\frac{E_N + M}{2E_N}} \sum_{\kappa, m_\ell, m} e^{-i\delta_\kappa^*}\, i^\ell \langle \ell\ m_\ell\ \tfrac{1}{2}\ s_N | j\ m\rangle Y_{\ell m_\ell}^*(\hat{p}_N)\psi_\kappa^{jm}(\boldsymbol{r})\,, \tag{2.46}$$

where $\psi_\kappa^{jm}(\boldsymbol{r})$ are four-spinors of the same form as that in Eq. (2.41), except that now the radial functions $f_\kappa$, $g_\kappa$ are complex because of the complex optical potential. It should also be mentioned that since the wave function (2.46) corresponds to an outgoing nucleon, we use the complex conjugates of the radial functions and phase shifts (the latter with the minus sign).

To obtain the cross-section we integrate analytically over all possible (unobserved) angles for the outgoing nucleon. The remaining integrations (on the kinematical variables of the unobserved final lepton) are performed numerically. Notice that this procedure differs from the one adopted in the RFG, where the kinematical variables of the final lepton is integrated first.

*2.3. Nucleonic form factors*

In a previous work [3] concerning the asymmetry (1.1) in the context of elastic $\nu(\bar{\nu})$-nucleon scattering, the influence of different parameterizations of the electromagnetic form factors has been carefully analyzed, being one of the sources of uncertainty in disentangling the presence of strange form factors at intermediate/large $Q^2$ values. In particular the magnetic form factors are the only ones entering into play in the differences of neutrino and anti-neutrino cross sections and Ref. [3] shows, in the analysis of (1.1), a non-negligible error band due to the present experimental uncertainty in the measurements of magnetic form factors (specifically the ones of the neutron).

In the present work we intend to evaluate not only the above mentioned asymmetry, but also the separate cross sections which enter into its definition: thus both electric and magnetic nucleonic form factors enter into the definition of the vector and magnetic weak NC and CC form factors.

We are interested in values of the form factors at relatively small $Q^2$ ($Q^2 \leqslant 1$ GeV$^2$): in this region the standard dipole parameterization of the electromagnetic form factors $G_E^p$, $G_M^p$ and $G_M^n$ (with a dipole mass $M_V = 0.84$ GeV) and the Galster parameterization [34] for the neutron electric form factor, $G_E^n$, provide a fair description of the experimental data [35].

For simplicity the usual dipole form has also been used for the axial nucleonic form factor, $F_A$, with a cutoff mass $M_A = 1.032$ GeV. Moreover the pseudoscalar form factor $F_P^{CC}$, entering into the CC cross sections, is taken as it is given by PCAC and pion dominance [36]:

$$F_P^{CC}(Q^2) = -\frac{2M}{m_\pi^2 + Q^2} F_A^{CC}(Q^2) \,, \tag{2.47}$$

$m_\pi$ being the pion mass.

There remain to be considered an explicit form for the strange form factors entering into the NC weak nucleonic current: we shall use here the following dipole forms:

$$G_M^s(Q^2) = \frac{\mu_s}{(1 + Q^2/M_V^2)^2} \,, \tag{2.48}$$

$$F_A^s(Q^2) = \frac{g_A^s}{(1 + Q^2/M_A^2)^2} \,, \tag{2.49}$$

with typical values for $g_A^s$ and $\mu_s$, which will be discussed later. Alternative $Q^2$ dependencies of these form factors have been considered in Ref. [3] and could be employed here as well, with similar outcomes.

## 3. Results and discussion

In this section we shall present the results of our calculations for $\nu(\bar{\nu})$-nucleus cross sections using both nuclear models described above; in addition to separate cross section,

we will also consider the ratio between $(\nu, p)$ and $(\nu, n)$ NC cross sections: [4]

$$R_{p/n} = \frac{\left(d\sigma/dT_N\right)^{NC}_{(\nu,p)}}{\left(d\sigma/dT_N\right)^{NC}_{(\nu,n)}}, \tag{3.1}$$

Moreover we shall evaluate a quantity analogous to Eq. (1.1) for the case of inelastic cross sections:

$$\mathcal{A}_N(T_N) = \frac{\left(d\sigma/dT_N\right)^{NC}_{(\nu,N)} - \left(d\sigma/dT_N\right)^{NC}_{(\bar{\nu},N)}}{\left(d\sigma/dT_N\right)^{CC}_{(\nu,p)} - \left(d\sigma/dT_N\right)^{CC}_{(\bar{\nu},n)}}, \tag{3.2}$$

$T_N$ being, as usual, the kinetic energy of the ejected nucleon (proton or neutron).

The shell model calculations have been done for the $^{12}$C nucleus, while in the Fermi Gas model we employ a Fermi momentum $p_F = 225$ MeV/c, which is supposed to account for the average density of $^{12}$C (smaller than the ordinary nuclear matter density).

We start by considering a relatively "low" incoming neutrino energy, $E_\nu = 200$ MeV, which is a typical value for the beam of neutrinos from decay in flight available at LAMPF [11]: Figs. 4a,b show the $\nu(\bar{\nu})+A \rightarrow \nu(\bar{\nu})+p+(A-1)$ (a) and $\nu_\mu(\bar{\nu}_\mu)+A \rightarrow \mu^-(\mu^+)+p(n)+(A-1)$ (b) cross sections, Eq. (2.18), evaluated with the RFG model without ($\epsilon_B = 0$) and with ($\epsilon_B = -25$ MeV) binding energy for the hole states, as well as with the RSM formalism (which accounts for the experimental binding of the occupied states). Strange form factors are set to be zero. One can see rather large discrepancies between the various curves; when the average binding is taken into account in the RFG, the latter approaches the RSM cross sections, though there remain differences of the order of 10% or more.

A separate discussion is required by the inclusion of the appropriate corrections on the propagation of the final particles, namely the interaction of the ejected nucleon with the residual nucleus (FSI) and the Coulomb interaction of the final muon, for the CC processes. We remind here that there is a Coulomb correction also for an ejected proton, and this is taken into account in the Optical Potential, together with the effects of strong interactions.

A sizable reduction of the $\nu - A$ cross sections is induced by the FSI of the ejected nucleon, as it can be seen in Fig. 5 for the $\nu + A \rightarrow \nu + p + (A - 1)$ process: here the effect of the relativistic optical model potential turns out in a reduction of more than 50% as compared with the corresponding PWIA calculation. Similar results are found when the ejected nucleon is a neutron. Together with the ROP of Eqs. (2.44) and (2.45), we have also employed an optical potential based on the same mesonic model which describes the initial nuclear bound states: it provides a slightly smaller reduction than ROP, but gives a fair description of the main effects of the FSI; the comparison between the two optical potentials accounts for the theoretical uncertainty which one can ascribe to this part of the process.

---

[4] In this section the labels of the cross sections explicitly indicate the ejected, final particle (proton, neutron or generic nucleon).
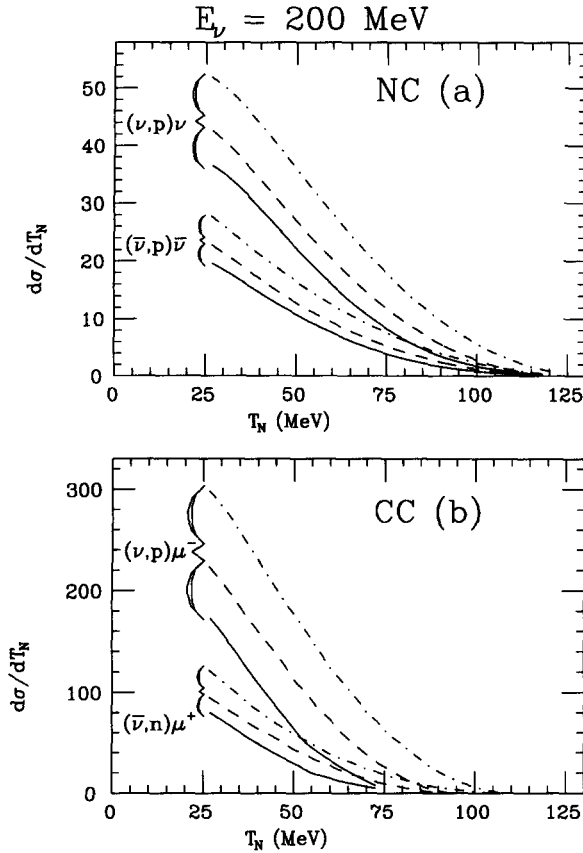
Fig. 4. The NC (a) and CC (b) differential cross sections for neutrino and anti-neutrino induced processes, versus the kinetic energy of the ejected nucleon, $T_N$, at incident $\nu(\bar{\nu})$ energy $E_\nu = 200$ MeV. The solid lines represent the RSM calculation, the dashed (dot dashed) lines are the results obtained with the RFG with $\epsilon_B = -25$ MeV ($\epsilon_B = 0$, respectively). Here and in the following the differential cross sections are in $10^{-42}$ cm$^2$ MeV$^{-1}$.

Concerning the Coulomb distortion on the final $\mu^\pm$ in the CC process, we have found that, at 200 MeV incident neutrino energy, this correction produces a increase from 5 to 19% in the $(\nu_\mu, \mu^-)$ cross sections and an decrease from 4 to 14% in the $(\bar{\nu}_\mu, \mu^+)$ ones, depending upon the outgoing nucleon energy. Thus the correction associated with the Coulomb interaction of the charged lepton is not negligible.

It is worth noticing that at this low neutrino energy the evaluation of the asymmetry (3.2) does not seem to be of particular interest, for at least two reasons: i) the dependence upon the nuclear model employed for the calculation of the separate cross sections remains quite large in the asymmetry, thus preventing the use of (3.2) to distinguish between different strangeness contents; ii) the energy range (in $T_N$) in which the ratio between NC and CC differences of cross sections is fairly stable (constant) is quite small ($\leqslant 20$–30 MeV). This last point is due to the muon mass, which rapidly brings the CC cross sections down to zero, contrary to what happens in the NC cross sections.
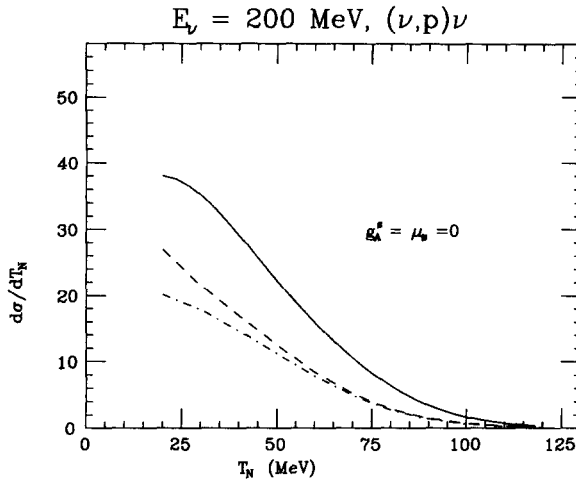
$$E_\nu = 200 \text{ MeV}, (\nu,p)\nu$$



Fig. 5. The NC differential cross sections for neutrino induced processes, versus $T_N$, at incident $\nu(\bar{\nu})$ energy $E_\nu = 200$ MeV. The solid line represents the RSM calculation within the PWIA; the other curves include the effects of FSI: with a meson-exchange Optical Potential (dashed line) and with the phenomenological ROP (dot-dashed line). No strange form factors are included.
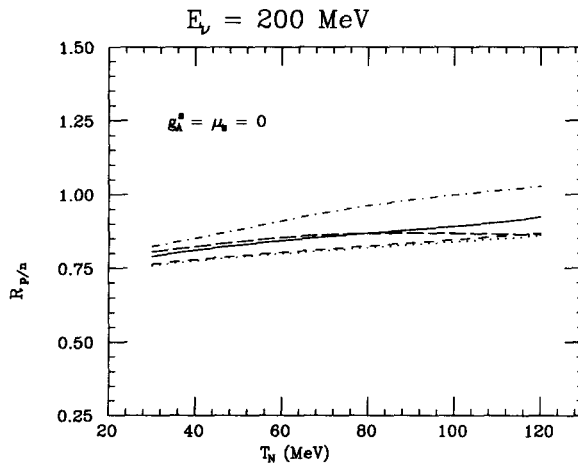
$$E_\nu = 200 \text{ MeV}$$



Fig. 6. The ratio $R_{p/n}$ for NC neutrino processes, versus $T_N$, at incident energy $E_\nu = 200$ MeV. The solid line is the pure RSM calculation, the dashed (dotted) lines are obtained with the RFG with $\epsilon_B = -25$ MeV ($\epsilon_B = 0$, respectively); the dot-dashed line corresponds to the RSM with FSI accounted for by the ROP model, while the long-dashed line is obtained by switching off the Coulomb interaction in the ROP. No strange form factors are included.

Then we have calculated the ratio of NC $\nu$-induced cross sections with a proton and a neutron in the final state, Eq. (3.1). This quantity was first suggested as a probe for strange form factors in Ref. [37,38]. It is shown first in Fig. 6 without strange form factors, again for an incoming neutrino energy of 200 MeV: in this figure we want to display the sensitivity of $R_{p/n}$ to the nuclear model description, both in the initial and in the final states. These results deserve the following comments:

i) Within the PWIA a small difference (of the order of 6–7%) remains between the shell model calculation and the free Fermi gas one, which in turn is much less affected by the average binding energy, as compared to the situation in Figs. 4a,b. These findings are in agreement with the calculations of Barbaro et al. [15], where the RFG is compared with predictions of the so-called Hybrid Model (again an independent particle approach).

ii) The inclusion of FSI, using the ROP model, leads to a sizable increase of $R_{p/n}$, the correction becoming larger with increasing energies; of course both $\sigma_{\nu,p}$ and $\sigma_{\nu,n}$ are strongly reduced by the FSI, but by a different amount. Indeed it might be interesting to notice that, by artificially switching off the Coulomb potential in (2.43), the correction of the FSI on the ratio $R_{p/n}$ becomes much smaller, being confined within about 4% with the exception of the largest values of $T_N$. Of course this does not imply that the Coulomb term is the most important in the optical model potential, since the main effects are ascribed to the strong interaction; the latter, however, due to isospin invariance, are similar on protons and neutrons and tend to cancel in the ratio of the cross sections, while the Coulomb correction does not; the point we wish to stress here is the necessity to take into account carefully any "Coulomb distortion" on the ejected proton.

As a final comment on this figure, we wish to compare with the results of Garvey et al. [38]; they evaluate the cross sections within a continuum random phase approximation (RPA) model, the initial nuclear (ground) state being a Slater determinant of Woods–Saxon single particle wave functions. The RPA correlations provide a microscopic description of the FSI, while in our case the FSI are embodied in the phenomenological optical potential, and we only consider one-nucleon emission. Even though both ways of treating FSI are very different, once the ratio $R_{p/n}$ is considered, the two approaches lead to similar conclusions, stressing once more the stability of this quantity against differences in the nuclear models employed.

The modification of the ratio $R_{p/n}$ induced by the presence of strange form factors is illustrated in Fig. 7, where the shell model calculations both in PWIA and DWIA (evaluated with the full ROP) are reported. We compare the ratio obtained in the absence of strangeness ($g_A^s = \mu_s = 0$) with two cases: one with $g_A^s = -0.15$ and $\mu_s = 0$, the second with $g_A^s = -0.15$ and $\mu_s = -0.3$. It is clearly seen that the effects of strangeness are quite sizable, particularly the ones associated with $g_A^s$; the deviations induced by the magnetic strange form factor are smaller and comparable with the non-negligible correction produced by the FSI.

We notice that in Ref. [15] the nuclear model theoretical uncertainty on $g_A^s$ deduced from the ratio $R_{p/n}$ is also found to be fairly small, of the order of $\delta_{nuc}(g_A^s) = \pm 0.015$. In that work FSI are not taken into account, while off-shellness effects are estimated to be of the same order as the nuclear model uncertainty.

Thus, a measurement of $R_{p/n}$ should allow to disentangle altogether a contribution from strange form factors; this conclusion is in qualitative agreement with the results of Garvey et al. [38].

We turn now to analyze situations corresponding to higher incident neutrino energies; in particular we have considered $E_\nu = 500$ MeV and $E_\nu = 1$ GeV as typical values for
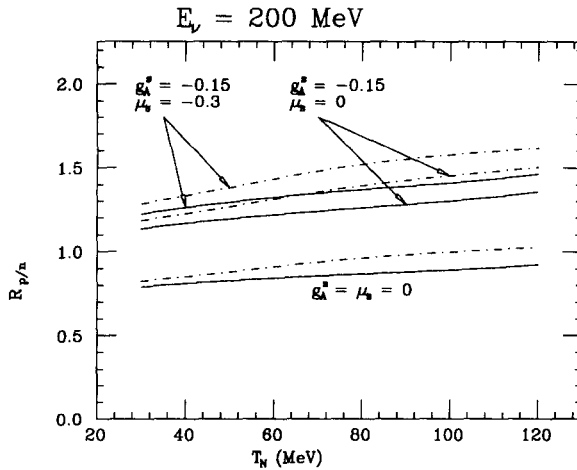
Fig. 7. The ratio $R_{p/n}$ for NC neutrino processes, versus $T_N$, at incident energy $E_\nu = 200$ MeV. The solid lines correspond to the RSM calculation, the dot-dashed lines include the effect of FSI accounted for by the ROP model; Three different choices of strangeness parameters are shown, as indicated in the figure.

the discussion of the nuclear effects on the asymmetry (3.2), which is the main focus of this work.

Figs. 8a,b show the separated cross sections for NC and CC processes at $E_\nu = 500$ MeV: the RSM (solid lines) is again compared (in PWIA) with the two "versions" of the RFG, with (dashed lines) and without (dot-dashed lines) binding energy: there remain some discrepancies between the two approaches, but limited within some 7% for the RFG with binding. The reduction of the cross sections induced by FSI (again incorporated by using the ROP within the shell model approach), instead, remains sizable (of the order of 40%), as it appears from the long-dashed lines.

For this value of $E_\nu$ it starts being of some interest to consider the asymmetry (3.2), which is illustrated in Fig. 9: here we compare $\mathcal{A}_p$ evaluated a) in the RFG with $\epsilon_B = -25$ MeV (dashed lines), b) in the RSM without FSI (solid lines) and in DWIA, with the FSI provided by the ROP (dot-dashed lines). The differences between the various models turn out to be quite reduced in the ratio defining the asymmetry, with respect to the corresponding effects on the separated cross sections. The largest correction (within 8%) remains the one associated to the FSI.

The finite muon mass, which, as already noticed above, brings the CC cross sections down to zero at lower $T_N$ values with respect to the NC ones, produces a rapid increase of the asymmetry for $T_N \geqslant 150$ MeV, thus leaving a reasonable energy range ($50 \leqslant T_N \leqslant 150$ MeV) in which the asymmetry has a fairly constant value. Therefore it is worth comparing the results for the asymmetry, obtained with different estimates for the parameters $(g_A^s, \mu_s)$ of the strange form factors: Fig. 9 shows that a measurement of the asymmetry could appreciably reveal the existence of non-vanishing axial and/or magnetic strange form factors. Indeed the differences in $\mathcal{A}_N$ associated with, e.g. a value of $g_A^s = -0.15$ amount to about 15%, which is outside the "theoretical uncertainty" provided by the excursion in $\mathcal{A}_N$ values obtained with different nuclear models.
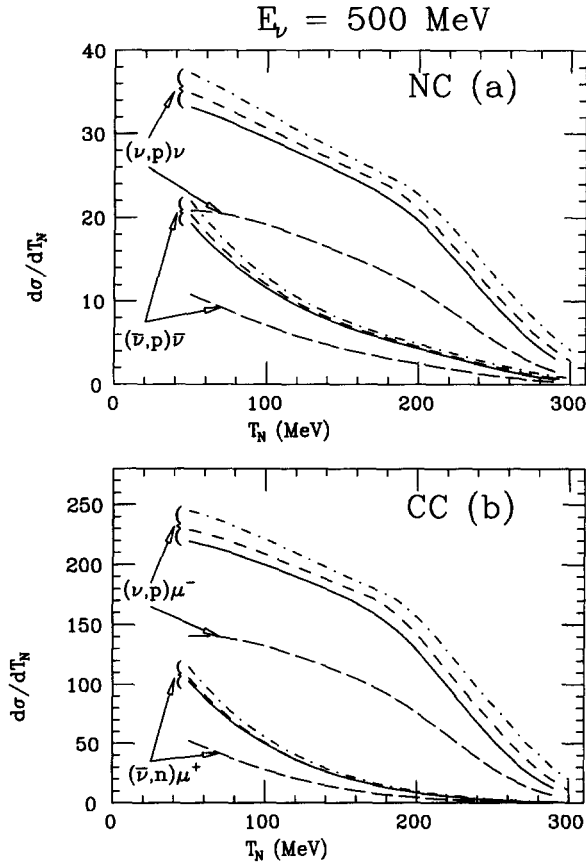
$$E_\nu = 500 \text{ MeV}$$



Fig. 8. The NC (a) and CC (b) differential cross sections for neutrino and anti-neutrino induced processes, versus the kinetic energy of the ejected nucleon, $T_N$, at incident $\nu(\bar{\nu})$ energy $E_\nu = 500$ MeV. The solid lines represent the RSM calculation in PWIA, the dashed (dot dashed) lines are the results obtained with the RFG with $\epsilon_B = -25$ MeV ($\epsilon_B = 0$, respectively), again in PWIA. The long-dashed lines are the RSM calculation in DWIA, using the ROP.

Similar considerations apply to the $E_\nu = 1$ GeV case (and to higher neutrino energies): here, however, it is worth noticing that already for the separated cross sections the differences between RFG and RSM turn out to be negligible, while the reduction produced by the FSI remains sizable. This reduction, due to the imaginary term of the optical potential, takes into account that only $\simeq 50\%$ of the events correspond to the quasielastic channel. This is in rough agreement with a Monte Carlo simulation and experimental observations [39]. The FSI produces, as expected, a much smaller effect on the asymmetry, as it is illustrated in Fig. 10: only the calculations within the RSM (without and with FSI) are shown in the figure, since the corresponding curves obtained within the RFG model would practically coincide with the ones displayed in the figure. The FSI produce a correction of the order of few (4–5) %, but for the smallest $T_N$ values, while the effects of non-vanishing strange form factors is quite larger. Moreover we display the results obtained by taking into account, in addition to the FSI, also the
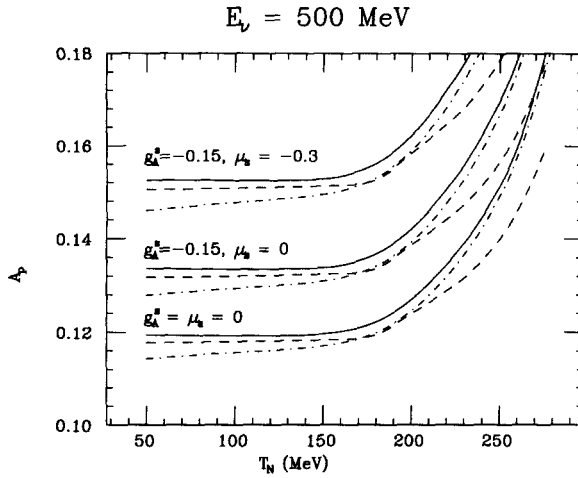
$$E_\nu = 500 \text{ MeV}$$



Fig. 9. The asymmetry (3.2), $\mathcal{A}_p$ for an ejected proton, versus $T_N$, at incident $\nu(\bar{\nu})$ energy $E_\nu = 500$ MeV. The solid lines correspond to the RSM calculation, the dashed lines to the RFG with $\epsilon_B = -25$ MeV and the dot-dashed lines are in DWIA evaluated with ROP model. The three set of curves correspond to different choices of strangeness parameters: $g_A^s = \mu_s = 0$ (lower lines), $g_A^s = -0.15$, $\mu_s = 0$ (intermediate lines) and $g_A^s = -0.15$, $\mu_s = -0.3$ (upper lines).
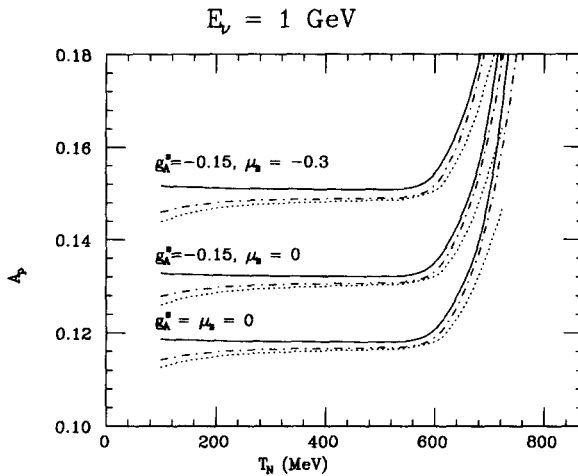
$$E_\nu = 1 \text{ GeV}$$



Fig. 10. The asymmetry (3.2), $\mathcal{A}_p$ for an ejected proton, versus $T_N$, at incident $\nu(\bar{\nu})$ energy $E_\nu = 1.0$ GeV. The solid lines correspond to the RSM calculation, the dot-dashed lines are in DWIA evaluated with ROP model, the dotted lines represent the RSM corrected by the the FSI and the Coulomb distortion of the muon in the CC processes in the denominator of $\mathcal{A}_p$. The three sets of curves correspond again to different choices of strangeness parameters: $g_A^s = \mu_s = 0$ (lower lines), $g_A^s = -0.15$, $\mu_s = 0$ (intermediate lines) and $g_A^s = -0.15$, $\mu_s = -0.3$ (upper lines).

Coulomb distortion of the final muon in the denominator of (3.2). The corresponding correction (with respect of the PWIA) is smaller than the one associated with FSI, both of them resulting in a reduction of the asymmetry. The global effect of FSI+Coulomb distortion does not exceed about 6% (again with the exception of the smallest $T_N$ values). In any case the effects of the strange form factors remain well distinguished with
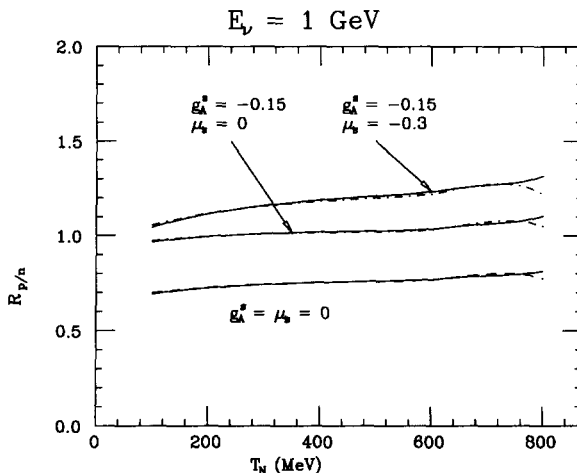
$$E_\nu \; = \; 1 \; GeV$$



Fig. 11. The ratio $R_{p/n}$ for NC neutrino processes, versus $T_N$, at incident energy $E_\nu = 1$ GeV. The solid lines correspond to the RSM calculation, the dot-dashed lines include the effect of FSI accounted for by the ROP model; Three different choices of strangeness parameters are shown, as indicated in the figure.

respect to the nuclear medium corrections.

On the basis of the results obtained for $E_\nu = 1$ GeV, we can also state that for higher neutrino energies the RFG model (corrected by FSI and Coulomb distortion) can be safely employed to compare with the experiment: indeed, as expected, the shell structure effects have no influence when the energy/momentum transferred to the target nucleus are much larger than the binding of nucleons inside. Moreover, at these high energy and momentum transfers, collective effects and long range correlations are not expected to play an important role (see, for example, Ref. [38]).

Therefore we can conclude that for incident neutrino energies larger than 1 GeV our calculations indicate that the influence of nuclear models on the neutrino asymmetry $\mathcal{A}_N$ is rather modest and well under control: this is an important (although expected) outcome, since it implies that the sensitivity of (3.2) to the unknown components of the nucleonic form factors is comparable to the one discussed for the elastic scattering [3]. The real difference between the two situations concerns the measurable kinematic variables, in particular the fact that $Q^2$ is no longer fixed. It would be interesting to study whether this asymmetry is also insensitive to other nuclear medium effects such as off-shellness of the bound nucleons, not considered here. If this is confirmed the asymmetry measured via inelastic scattering on nuclei (which is the most common experimental situation) could allow, as well as in the elastic processes, to disentangle the strange components of the nucleonic weak form factors.

We considered it worthwhile to evaluate, for $E_\nu = 1$ GeV, also the ratio $R_{p/n}$; indeed this neutrino energy is close to the one of a previous elastic scattering experiment performed in Brookhaven and analyzed by Garvey et al. in connection with the strange axial constant [2]. In Fig. 11 we display the ratio (3.1) evaluated with the RSM, both in PWIA (solid lines) and in DWIA (dot-dashed lines), utilizing the ROP.
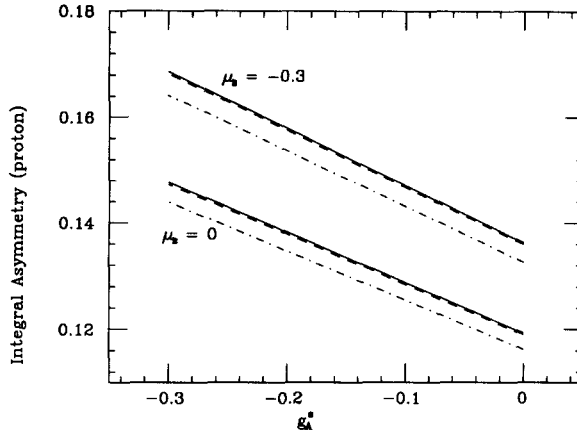
Fig. 12. The integral asymmetry (3.3), $\mathcal{A}_p^I$ for an ejected proton, versus $g_A^s$, at incident $\nu(\bar{\nu})$ energy $E_\nu = 1.0$ GeV. The solid lines correspond to the RSM calculation, the dashed lines to the RFG with average binding energy $\epsilon_B = -25$ MeV, the dot-dashed lines to the DWIA evaluated with RSM and ROP model. The two sets of curves correspond to different choices of the magnetic strangeness parameter: $\mu_s = 0$ (lower lines) and $\mu_s = -0.3$ (upper lines).

The differences between the two approaches turn out to be fairly negligible, while the effect of different values for the strangeness parameters $g_A^s$ and $\mu_s$ (we use here the same three choices employed in Fig. 7) is quite large. In contrast to the $E_\nu = 200$ MeV case, nuclear model effects do not appreciably alter this ratio, whereas the strange components of the nucleonic form factors produce corrections, for example, of more than 30% when $g_A^s$ varies from 0 to $-0.15$, thus compelling toward a direct measurement of this quantity.

Concerning the $Q^2$ dependence of the form factors, we have not discussed here the influence of different parameterizations of the electromagnetic and axial form factors entering into the calculation. Indeed we have employed in the present work the usual dipole parameterization both for non-strange and strange form factors, keeping as free parameters only the strengths ($g_A^s$ and $\mu_s$) of the latter. Due to the close similarity of the present results (for $E_\nu \gtrsim 1$ GeV) to the ones obtained, for the asymmetry, in the elastic case [3], one should keep in mind that the uncertainties in the electromagnetic form factors, discussed there at length, will also affect the asymmetry defined in the inelastic neutrino-nucleus scattering: as in the previous case, however, their entity should not spoil the possibility of disentangling the effects of strangeness.

Finally we consider a quantity which can be defined as "integral asymmetry" and is obtained from the ratio of NC and CC differences between total cross sections [see Eq. (2.19) ]:

$$\mathcal{A}_N^I = \frac{\sigma_{\nu N}^{NC} - \sigma_{\bar{\nu} N}^{NC}}{\sigma_{(\nu,p)}^{CC} - \sigma_{(\bar{\nu},n)}^{CC}} . \tag{3.3}$$

The integral asymmetry is displayed in Fig. 12 for $E_\nu = 1$ GeV, as a function of the axial strangeness parameter, $g_A^s$, and for two different choices of the strange magnetic moment $\mu_s$ (0 and $-0.3$). The calculation of $\mathcal{A}_p^I$ has been performed both in PWIA

(with the RFG and the RSM) and in DWIA (using the ROP): although this quantity is obtained by integrating over the ejected nucleon energy (and thus over the final state), the effect of FSI still shows up in a reduction of about 4% of the integral asymmetry. However, the sensitivity of $\mathcal{A}_p^l$ to the strangeness parameters is much larger than to the nuclear model effects. The correlation between $g_A^s$ and $\mu_s$ is clearly displayed in Fig. 12.

In conclusion, the present analysis shows that quasi-elastic neutrino–nucleus scattering can be conveniently utilized to look for evidence of non-vanishing strange nucleonic form factors; we have found that both the ratio $R_{p/n}$ and the nuclear asymmetry (3.2) are appropriate quantities to be considered, as they are fairly sensitive to the strangeness parameters.

## Acknowledgements

## References

[1] D.B. Kaplan and A. Manohar, Nucl. Phys. B 310 (1988) 527;
    J. Ellis and M. Karliner, Phys. Lett. B 213 (1988) 73.
[2] G.T. Garvey, W.C. Louis and D.H. White, Phys. Rev. C 48 (1993) 761.
[3] W.M. Alberico, S.M. Bilenky, C. Giunti and C. Maieron, Z. Phys. C 70 (1996) 463.
[4] J. Ashman et al., Phys. Lett. B 206 (1988) 364; Nucl. Phys. B 328 (1989) 1.
[5] D. Adams et al., Phys. Lett. B 329 (1994) 399.
[6] K. Abe et al., Phys. Rev. Lett. 74 (1995) 346.
[7] J. Ellis and M. Karliner, Phys. Lett. B 341 (1995) 397
[8] M. Anselmino, A. Efremov and E. Leader, Phys. Rep. 261 (1995) 1.
[9] J. Lichtenstadt and H.J. Lipkin, preprint TAUP-2244-95 (hep-ph@@xxx.lanl.gov/9504277).
[10] B. Mueller et al., (nucl-ex@@xxx.lanl.gov/9702004, February 1997).
[11] W.C. Louis, in Spin and Isospin in Nuclear Interactions, ed. S.W. Wissink, C. Goodman and G. Walker (Plenum, New York, 1991) p. 341.
[12] C.J. Horowitz, Hungchong Kim, D.P. Murdock and S. Pollock, Phys. Rev. C 48 (1993) 3078.
[13] Hungchong Kim, J. Piekarewicz and C.J. Horowitz, Phys. Rev. C 51 (1995) 2739
[14] S.K. Singh and E. Oset, Nucl. Phys. A 542 (1992) 587
[15] M.B. Barbaro, A. De Pace, T.W. Donnelly, A. Molinari and M.J. Musolf, Phys. Rev. C 54 (1996) 1954.
[16] J.M. Udías, P. Sarriguren, E. Moya de Guerra, E. Garrido, and J.A. Caballero, Phys. Rev. C 48 (1993) 2731.
[17] J.M. Udías, P. Sarriguren, E. Moya de Guerra, and J.A. Caballero, Phys. Rev. C 53 (1996) R1488.
[18] Y. Jin, D.S. Onley and L.E. Wright, Phys. Rev. C 45 1311 (1992).
[19] J. Jourdan, Nucl. Phys. A 603 (1996) 117; Phys. Lett. B 353 (1995) 189.
[20] C.R. Chinn and A. Picklesimer, Nuovo Cimento 105 A (1992) 1149.
[21] S. Frullani and J. Mougey, Adv. Nucl. Phys. 14 (1984) 1.
[22] W.M. Alberico, T.W. Donnelly and A. Molinari, Nucl. Phys. A 512 (1990) 541.
[23] H. Überall, in Electron Scattering from Complex Nuclei (Academic Press, New York, 1971).
[24] C. Giusti and F.D. Pacati, Nucl. Phys. A 473 (1987) 717.
[25] J.M. Udias, NIKHEF-K INternal Report, NIKHEF-95-P12.

[26] Y. Umino and J.M. Udias, Phys. Rev. C 52 (1995) 3399.
[27] C.J. Horowitz and B.D. Serot, Nucl. Phys. A 368 (1981) 503; Phys. Lett. B 86 (1979) 146;
C.J. Horowitz, D.P. Murdock, and B.D. Serot, *in* Computational Nuclear Physics, ed. K. Langanke, J.A. Maruhn, and S.E. Koonin (Springer, Berlin, 1991).
[28] B.D. Serot and J.D. Walecka, Adv. Nucl. Phys. 16 (1986) 1.
[29] P.-G. Reinhard et al., Z. Phys. A 323 (1986) 13; A 329 (1988) 257.
[30] Y.K. Gambhir, P. Ring and A. Thimet, Ann. Phys. 198 (1990) 132.
[31] J.M. Udías, Ph.D. Thesis, Universidad Autónoma de Madrid (1993).
[32] M.E. Rose, Relativistic Electron Theory (Wiley, 1961).
[33] S. Hama, B.C. Clark, E.D. Cooper, H.S. Sherif, and R.L. Mercer, Phys. Rev. C 41 (1990) 2737;
E.D. Cooper, S. Hama, B.C. Clark and R.L. Mercer, Phys. Rev. C 47 (1993) 297.
[34] S. Galster, Nucl. Phys. B 32 (1971) 221.
[35] Gerassimos G. Petratos, SLAC-PUB-6328, (Dec. 1993), *in* Proc. Electron nucleus scattering, Marciana Marina 1993, p. 21.
[36] C.H. Llewellyn Smith, Phys. Rep. 3 C, 261 (1971).
[37] G.T. Garvey, S. Krewald, E. Kolbe and K. Langanke, Phys. Lett. B 289 (1992) 249.
[38] G.T. Garvey, E. Kolbe, K. Langanke and S. Krewald, Phys. Rev. C 48 (1993) 1919.
[39] L.A. Ahrens et al., Phys. Rev. D 35 (1987) 785.